Solution structure of the antiapoptotic protein bcl-2

Andrew M. Petros*, Ales Medek*, David G. Nettesheim*, Daniel H. Kim*, Ho Sup Yoon*, Kerry Swift*, Edmund D. Matayoshi*, Tilman Oltersdorf†, and Stephen W. Fesik*‡

*Pharmaceutical Discovery Division, Abbott Laboratories, Abbott Park, IL 60064; and †IDUN Pharmaceuticals, La Jolla, CA 92037

Communicated by Stanley J. Korsmeyer, Dana–Farber Cancer Institute, Boston, MA, December 26, 2000 (received for review November 3, 2000)

The structures of two isoforms of Bcl-2 that differ by two amino acids have been determined by NMR spectroscopy. Because wild-type Bcl-2 behaved poorly in solution, the structures were determined by using Bcl-2/Bcl-x_L chimeras in which part of the putative unstructured loop of Bcl-2 was replaced with a shortened loop from Bcl-x_L. These chimeric proteins have a low pI compared with the wild-type protein and are soluble. The structures of the two Bcl-2 isoforms consist of 6 α-helices with a hydrophobic groove on the surface similar to that observed for the homologous protein, Bcl-x_L. Comparison of the Bcl-2 structures to that of Bcl-x_L shows that although the overall fold is the same, there are differences in the structural topology and electrostatic potential of the binding groove. Although the structures of the two isoforms of Bcl-2 are virtually identical, differences were observed in the ability of the proteins to bind to a 25-residue peptide from the proapoptotic Bad protein and a 16-residue peptide from the proapoptotic Bak protein. These results suggest that there are subtle differences in the hydrophobic binding groove in Bcl-2 that may translate into differences in antiapoptotic activity for the two isoforms.

Bcl-2 is the founding member of a family of proteins involved in cell death that was identified originally at the breakpoint of a t(14;18) translocation in a lymphocytic leukemia cell line (1–6). Bcl-2 and other members of the family play an important role in embryogenesis, tissue remodeling, and the immune response through their actions as either inhibitors or promoters of apoptosis (7–9). There are at least 16 Bcl-2 homologues found in humans (10). These include Bcl-2, Bcl-x_L, Bcl-w, and Mcl-1, which are inhibitors of cell death, and Bad, Bak, Bax, Bid, Bim, and Bcl-x_S, which are cell-death promoters. Homeostasis is maintained in normal tissues through the antagonistic interaction of these anti- and proapoptotic proteins (11).

In addition to their normal function, aberrant expression of Bcl-2 proteins has been linked to many diseases such as autoimmunity and neurodegenerative disorders and cancer (12–14). Indeed, Bcl-2 has been found to be overexpressed in many cancer cells, including most B cell-derived lymphomas, colorectal adenocarcinomas, and undifferentiated nasopharyngeal cancers (15). Bcl-2 has been implicated also in the resistance of many cancers to treatment with radiation and chemotherapeutic agents (10, 13). Therefore, Bcl-2 represents a target for the treatment of cancers, especially those in which Bcl-2 is overexpressed and for which traditional therapy has failed (15–19).

The design of molecules that bind to Bcl-2 and inhibit its antiapoptotic activity could be aided greatly by the three-dimensional structure of Bcl-2 and Bcl-2–ligand complexes. The structure of a homologous protein, Bcl-x_L, has been determined previously, both alone and complexed to proapoptotic peptides from Bak and Bad (20–22). Bcl-x_L is an all α-helical protein that resembles the membrane insertion domain of bacterial toxins such as diphtheria toxin and the colicins. In the structure of the uncomplexed protein, a 56-residue flexible loop was observed and found to be nonessential for antiapoptotic activity. Therefore, before determining to the structures of the Bcl-x_L–peptide complexes, this flexible loop was truncated from 56 to 16 residues. This change not only simplified the NMR spectrum of the protein but also improved the behavior of Bcl-x_L in solution.

Although Bcl-x_L and Bcl-2 share a high degree of sequence homology (Fig. 1.), they have different tissue distributions and are expressed differentially in cancers (23–29). For example, Bcl-2 seems to be the major inhibitor of cell death in acute myeloid leukemia, whereas overexpression of Bcl-x_L correlates with resistance to cell death in breast cancer. Bcl-2 and Bcl-x_L also differ in their binding specificities for proapoptotic members of the Bcl-2 family (30). These differences in binding specificity could be caused by structural differences between these two proteins.

GenBank contains several entries for Bcl-2 that differ by a small number of amino acids. Although the physiological relevance of these changes is unclear, two of these differences affect the predicted binding site for proapoptotic Bcl-2 family proteins: threonine or alanine in position 96 and glycine or arginine in position 110 (Fig. 1). Here we describe three-dimensional structures of two isoforms of Bcl-2, denoted Bcl-2(1) (1, 2) and Bcl-2(2) (3–6), in solution by NMR spectroscopy. The structures of the Bcl-2 proteins were compared with each other and to a previously determined structure of Bcl-x_L. To determine whether the two isoforms of Bcl-2 bind differently to proapoptotic peptides, the affinities of both Bcl-2 isoforms were measured for peptides derived from Bak and Bad.

Materials and Methods

Plasmid Construction. Several different Bcl-2 constructs were prepared and evaluated for their suitability for NMR structural studies. A fragment coding amino acids 1–218 of Bcl-2(1) (Fig. 1) was obtained from Daudi mRNA (CLONTECH) by reverse transcription (RT)–PCR using an RT PCR kit (Roche Molecular Biochemicals). The fragment was inserted into the *Nde*I and *Xho*I sites of the pET30b plasmid (Novagen) for expression. By using this plasmid as a template, three other plasmids were prepared. In each case, the *Nde*I and *Xho*I sites of pET28b were used in the new construction. The first plasmid contained a fragment coding amino acids 1–50 and 92–218 of Bcl-2(1). A second plasmid was constructed that contained a fragment coding amino acids 1–34 of Bcl-2(1), 35–50 of Bcl-x_L, and 92–218 of Bcl-2(1). The third plasmid contained a fragment coding amino acids 1–34 of Bcl-2(1), 35–50 of Bcl-x_L, and 92–207 of Bcl-2(1). For constructing the plasmid for isoform 2, this last plasmid was used as a DNA template. Alanine 96 and glycine 110 were changed to a threonine and arginine, respectively, by using the Stratagene Quick Change kit (Stratagene).

Expression and Purification. The Bcl-2 proteins were expressed in *Escherichia coli* BL21(DE3) grown in M9 medium containing $^{15}NH_4Cl$, $^{15}NH_4Cl$ plus [U-^{13}C]glucose or $^{15}NH_4Cl$, [U-^{13}C]glucose, and 75% ^2H_2O. For isoform 1, soluble protein was purified

Abbreviations: NOE, nuclear Overhauser effect; NOESY, NOE spectroscopy; RMSD, root-mean-square deviation.

Data deposition: The atomic coordinates have been deposited in the Protein Data Bank, www.rcsb.org (PDB ID codes 1G5M and 1G5O).

‡To whom reprint requests should be addressed at: Abbott Laboratories, 100 Abbott Park Road, D460, AP10, Abbott Park, IL 60064-6098. E-mail: stephen.fesik@abbott.com.

The publication costs of this article were defrayed in part by page charge payment. This article must therefore be hereby marked "*advertisement*" in accordance with 18 U.S.C. §1734 solely to indicate this fact.

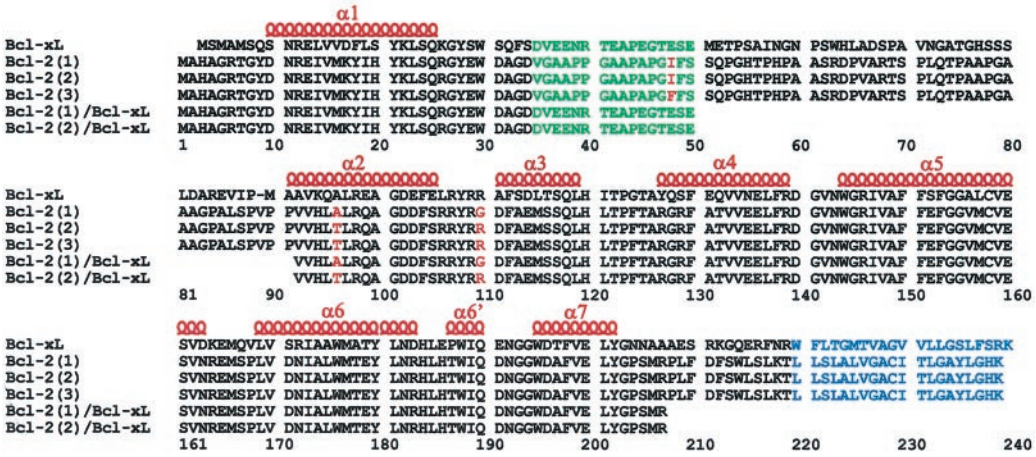

Fig. 1. Sequence alignment of full-length Bcl-x_L, the three isoforms of full-length Bcl-2 [denoted Bcl-2(1) (1,2), Bcl-2(2) (3,4), and Bcl-2(3) (5,6)], and the truncated Bcl-2/Bcl-x_L chimeras used in this study. Amino acid differences between the Bcl-2 isoforms are shown in red, the truncated loop is shown in green, and the putative membrane-spanning region is shown in blue. α-helices previously identified in Bcl-x_L are denoted above the sequence in red.

by Ni^{2+}-affinity chromatography. The amino terminal His tag was removed by cleavage with biotinylated thrombin according to the manufacturer's protocol (Novagen). The thrombin was removed by adding Streptavidin Agarose (Novagen) to the reaction mix, and the cleaved His tag and any uncleaved protein were removed by passing the mixture over another pre-equilibrated Ni^{2+} column. For isoform 2, the soluble fraction after cell lysis was loaded on a Q-Sepharose column, washed with a buffer containing 25 mM Tris·HCl (pH 8.0) and 1 mM DTT, and eluted with a linear gradient of 0–1 M NaCl. The eluted fractions containing the Bcl-2(2) protein were concentrated and loaded on a Superdex 75 gel-filtration column pre-equilibrated with a buffer containing 25 mM Tris·HCl (pH 8.0), 1 mM DTT, and 150 mM NaCl. NMR samples contained 0.5–1.0 mM protein in either 90% H_2O/10% D_2O or 100% D_2O, 20 mM Tris (pH 7.8), and 5 mM DTT.

NMR Spectroscopy. All NMR experiments were acquired at 298 K on a Bruker DRX500, DRX600, or DRX800 NMR spectrometer. Backbone ^1H, ^{13}C, and ^{15}N resonance assignments were achieved with [^{15}N,^{13}C,^2H (75%)] Bcl-2 by using a suite of deuterium-decoupled triple-resonance experiments [HNCA, HN(CO)CA, HN(CA)CB, HN(COCA)CB, HNCO, and HN(CA)CO] (31). The side-chain ^1H and ^{13}C NMR signals were assigned from HCCH-TOCSY experiments (32), and stereospecific assignments of the valine and leucine methyl groups were obtained from an analysis of the ^{13}C–^{13}C coupling patterns observed for biosynthetically directed fractionally ^{13}C-labeled Bcl-2 (33). Nuclear Overhauser effect (NOE) distance restraints were obtained from three-dimensional ^{15}N- and ^{13}C-edited NOE (NOESY) spectra (34, 35) acquired with a mixing time of 80 ms. Slowly exchanging amide protons were identified in an ^{15}N-heteronuclear single quantum correlation spectrum (HSQC) recorded immediately after exchanging the protein into a buffer prepared with D_2O. Residual dipolar couplings (HN-N and C'-C^α) were measured by using undecoupled versions of the HNCO experiment on [^{15}N,^{13}C,^2H (75%)] Bcl-2 in the presence of 17 mg·ml^{-1} Pf1 phage (36–38).

Structure Calculations. Bcl-2 structures were calculated by using a simulated annealing protocol (39) with the program CNX (Molecular Simulations, San Diego, CA). A square-well potential (F_{NOE} = 50 kcal·mol^{-1}) was used to constrain NOE-derived distances. Based on the cross-peak intensities, NOE-derived distance restraints were given upper bounds of 3.0, 4.0, 5.0, or 6.0 Å. Torsion angle restraints ϕ,ψ were generated from an analysis of the N, C', C^α, and H^α chemical shifts by using the TALOS program (40). A force constant of 200 kcal·mol^{-1}·rad^{-2} was applied to all torsional restraints. Explicit hydrogen bonds were included in α-helices only for residues observed to have slowly exchanging amide protons. The program PROCHECK was used to analyze the geometric quality of the calculated structures in the ensemble (41).

Peptide Binding. A fluorescence polarization-based competition assay was used to determine the relative affinity of a 25-residue peptide from human Bad (NLWAAQRYGRELRRMSDEFVDSFKK) and a 16-residue peptide from Bak (GQVGRQLAIIGDDINR) (SynPep, Dublin, CA) for both Bcl-2 isoforms. A modified Bad peptide labeled with 6-carboxyfluorescein-succinimidyl ester (FAM) was used as the probe in both cases [(5-FAM)-AAAAAQRYGRELRRMSDEFVDSFKK)]. Titrations were carried out on an Abbott clinical diagnostics instrument (IMx, FPIA mode) as described (22) with both protein and peptide in a buffer containing 120 mM sodium phosphate (pH 7.55), 0.01% bovine gamma globulin, and 0.1% sodium azide. Dissociation constants were determined from titration curves by using the analytical approach of Dandliker *et al.* (42) with the program MINSQ 4.03 (Micromath Scientific Software, Salt Lake City, UT).

Results and Discussion

Sample Preparation and Optimization. Structural studies on wild-type Bcl-2(1) have been hampered by the poor solubility of the protein. As a consequence of the poor physical properties of Bcl-2, no three-dimensional structure of Bcl-2 has been reported thus far. In contrast, a homologous protein, Bcl-x_L, behaves well in solution allowing its x-ray and NMR structures to be determined (20). One of the major differences in sequence between Bcl-x_L and Bcl-2 is in a region of Bcl-2 predicted to adopt a flexible, unstructured loop. For Bcl-x_L, this region of the protein is unnecessary for its antiapoptotic activity (20). To test whether this predicted loop region was responsible for the poor behavior of Bcl-2(1) in solution, a version of Bcl-2(1) was prepared in which residues 51–91 were deleted (21). Unfortunately, the loop-deleted form of Bcl-2 behaved like the wild-type protein and aggregated at high concentration. This finding is consistent with the results of Anderson *et al.*, in which a form of Bcl-2 with the putative unstructured loop replaced by four alanines was not soluble enough for structural studies (43).

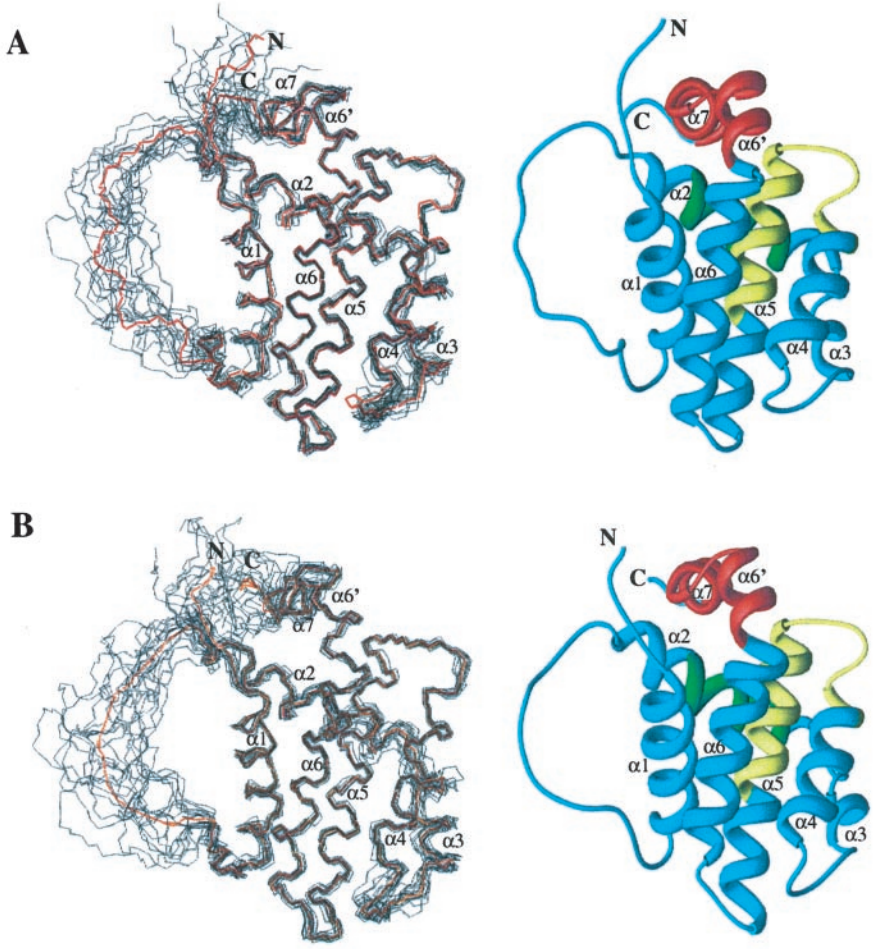

Fig. 2. (*A*) Backbone (N, Cα, C′) superposition of 15 low-energy NMR-derived structures and Ribbons (47) depiction of the average minimized structure for Bcl-2(1). (*B*) Backbone (N, Cα, C′) superposition of 15 low-energy NMR-derived structures and Ribbons depiction of the average-minimized structure for Bcl-2(2). For the superpositions, the mean structure is shown in red. Helices are numbered with respect to those observed in the structure of Bcl-x_L (20).

One possible reason for the poor solubility of the loop-deleted form of Bcl-2(1) was its unfavorable isoelectric point (6.4) that is very close to the pH of the buffer used in the NMR experiments and different from the pI of Bcl-x_L (4.9). This difference in isoelectric point, which could explain the variable solubilities of these proteins, stems largely from the greater number of anionic residues in Bcl-x_L (Fig. 1). To test this hypothesis, a chimeric protein was prepared in which the loop in Bcl-2 was replaced with the negatively charged loop of Bcl-x_L. This protein is predicted to have a much lower pI (5.0) and therefore should be more soluble. Although this chimeric protein behaved much better than the original construct and remained soluble up to 1 mM, ^{15}N, T_2 measurements suggested that the protein was still aggregating. Preliminary NMR experiments with this protein suggested that the eleven C-terminal residues, which contained several hydrophobic amino acids, were unstructured in solution and may be responsible for inducing the aggregation. Therefore, a second Bcl-2(1)/Bcl-x_L chimera was prepared in which these eleven C-terminal residues were removed (Fig. 1). Unlike the other forms of Bcl-2, this protein was very soluble and well behaved in solution. Moreover, the biological activity of this protein was retained as evidenced by the protection it provided against staurosporine-induced apoptosis when electroporated into Jurkat cells (data not shown).

The isoform 2 chimera was prepared from Bcl-2(1) by mutating residue 96 from an alanine to a threonine and mutating residue 110 from a glycine to an arginine. Bcl-2(2) also behaved well in solution and was suitable for structure determination by NMR.

Quality of the Bcl-2 Structures. Protein structures were calculated based on a total of 2,310 nontrivial NMR-derived distance restraints for isoform 1 and 2,337 nontrivial distance restraints for isoform 2. Fig. 2 shows the ensemble of 15 low-energy structures calculated with the program CNX for both isoforms. Excluding the flexible loop between helix 1 and helix 2 (residues 33–91), the eight N-terminal residues, and the four C-terminal residues, the root-mean-square deviation (RMSD) for Bcl-2(1) about the mean position is 0.59 Å for the backbone and 1.10 Å for all heavy atoms. For the same region in Bcl-2(2), the RMSD about the mean position is 0.61 Å for the backbone and 1.15 Å for all heavy atoms. The structural statistics for each ensemble and the energy-minimized average structures are given in Table 1. There are no distance violations greater than 0.4 Å or dihedral-angle violations greater than 5°. In the structure refinement, only covalent geometry, NOE, torsion, and repulsive van der Waals terms were included. Even so, the Lennard–Jones energy is large and negative, indicating that the structures have favorable nonbonded contacts. Analysis of the average-minimized structures with the program PROCHECK (41) showed that 78.3 and 77.1% of the residues of Bcl-2(1) and Bcl-2(2), respectively, lie in the most favored region of the Ramachandran plot, and 19.6 and 22.9% lie in the allowed regions.

Table 1. Structural statistics for Bcl-2 isoforms

		Bcl-2(1)			Bcl-2(2)	
Rmsd from experimental distance restraints, Å	Number of restraints	⟨SA⟩*	$\langle SA\rangle_r$	No. of restraints	⟨SA⟩	$\langle SA\rangle_r$
Long	651	0.008 ± 0.002	0.005	661	0.008 ± 0.002	0.007
Short	514	0.007 ± 0.002	0.003	544	0.010 ± 0.002	0.009
Sequential	554	0.009 ± 0.003	0.005	553	0.016 ± 0.002	0.012
Intra	591	0.008 ± 0.003	0.006	579	0.010 ± 0.004	0.007
H-Bonds	86	0.014 ± 0.002	0.010	62	0.014 ± 0.002	0.009
Talos	182			192		
CNX potential energies (kcal·mol^{-1})						
E_{total}		116.0 ± 4.7			160.7 ± 5.2	
E_{bonds}		3.9 ± 0.4			4.2 ± 0.5	
E_{angles}		62.2 ± 2.3			66.4 ± 2.3	
E_{vdw}		13.8 ± 1.5			13.9 ± 1.8	
E_{impr}		6.7 ± 0.6			7.8 ± 0.7	
E_{NOE}		8.9 ± 1.7			16.7 ± 3.4	
E_{cdih}		0.9 ± 0.4			0.7 ± 0.2	
E_{sani}		19.9 ± 2.9			50.9 ± 3.4	
E_{L-J}		−884 ± 10			−891 ± 13	
Rmsd, Å		Backbone	All heavy atoms	Backbone	All heavy atoms	
⟨SA⟩ vs. $\langle SA\rangle_r$		0.59 ± 0.11	1.10 ± 0.11	0.61 ± 0.09	1.15 ± 0.10	

*⟨SA⟩ is the ensemble of the 15 lowest energy structures, $\langle SA\rangle_r$ is the energy-minimized mean structure.

Description of Bcl-2 Structures. The overall structure of Bcl-2(1) consists of two central, predominately hydrophobic helices (helix 5 and 6) packed against four amphipathic α-helices (Fig. 2). Helix 1 (residues 11–24) is connected to helix 2 (residues 93–108) by a shortened artificial loop derived from Bcl-x_L. This loop is unstructured in solution as evidenced by the lack of medium and long-range NOEs for this region. Helix 1 and 2 are oriented parallel to one another, crossing at an angle of about 45°. A long loop, which contains a single turn of 3_{10} helix, connects helix 2 to helix 4 (residues 126–137) and results in a nearly orthogonal orientation for these two helices. Helices 4, 5 (residues 144–163), and 6 (residues 167–192) are oriented in a nearly antiparallel fashion with a kink in helix 6 at histidine 184. An irregular turn composed of two glycine residues connects helix 6 to helix 7 (residues 195–202), which orients helix 7 orthogonal to helices 4, 5, and 6.

A hydrophobic groove is present on the surface of the protein (Fig. 3). The analogous hydrophobic groove in Bcl-x_L corresponds to the region of the protein that binds to proapoptotic members of the Bcl-2 family. In Bcl-2, mutations in this region have been shown to abolish the antiapoptotic activity of Bcl-2 and block heterodimerization with other family members (44). Although Bcl-2(1) has a net negative charge at neutral pH, the charge distribution around the hydrophobic groove is balanced as shown in the GRASP (45) image of Fig. 4*A*.

The structure of isoform 2 is identical essentially to that of isoform 1 (Fig. 5). Excluding the residues of the flexible loop and the amino and carboxy termini, the backbone RMSD between the two structures is 1.10 Å. The substitution in isoform 2 of a threonine for an alanine at position 96 and an arginine for glycine at position 110 had no effect on the conformation of the protein within the experimental error of the structure determination. To assess potential differences between the binding grooves of these two proteins further, their affinities for a 16-residue peptide from the proapoptotic protein Bak and a 25-residue peptide from the proapoptotic protein Bad were measured in a fluorescence-based polarization assay (Table 2). Surprisingly, Bcl-2(2) binds the Bad peptide approximately 2-fold more tightly than Bcl-2(1), and it binds the Bak peptide about 8-fold more tightly. Thus, despite the similarity in their structures, the two isoforms display differences in their specificity for binding proapoptotic members of the Bcl-2 family.

Structural Comparison of Bcl-2 and Other Family Members. The NMR structures of Bcl-2(1) and Bcl-2(2) are compared with the previously determined NMR structure of Bcl-x_L (20) in Fig. 6. The overall folds are very similar to a backbone RMSD between Bcl-2(1) and Bcl-x_L of 1.91 Å and between Bcl-2(2) and Bcl-x_L of 1.84 Å (excluding the truncated loop). The largest difference is observed in the region of helix 3 that makes up part of the binding site. Excluding helix 3 (residues 110–125), the RMSD

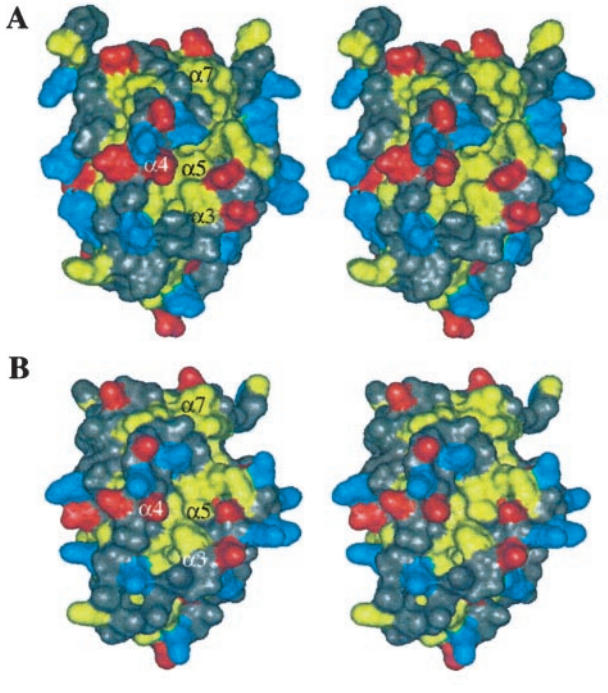

Fig. 3. Solvent-accessible surface showing hydrophobic groove for Bcl-2(1) (*A*) and Bcl-2(2) (*B*). Leucine, isoleucine, valine, tyrosine, phenylalanine, and tryptophan residues are colored yellow, aspartate and glutamate are colored red, and lysine, arginine, and histidine are colored blue. All other residue types are colored gray.

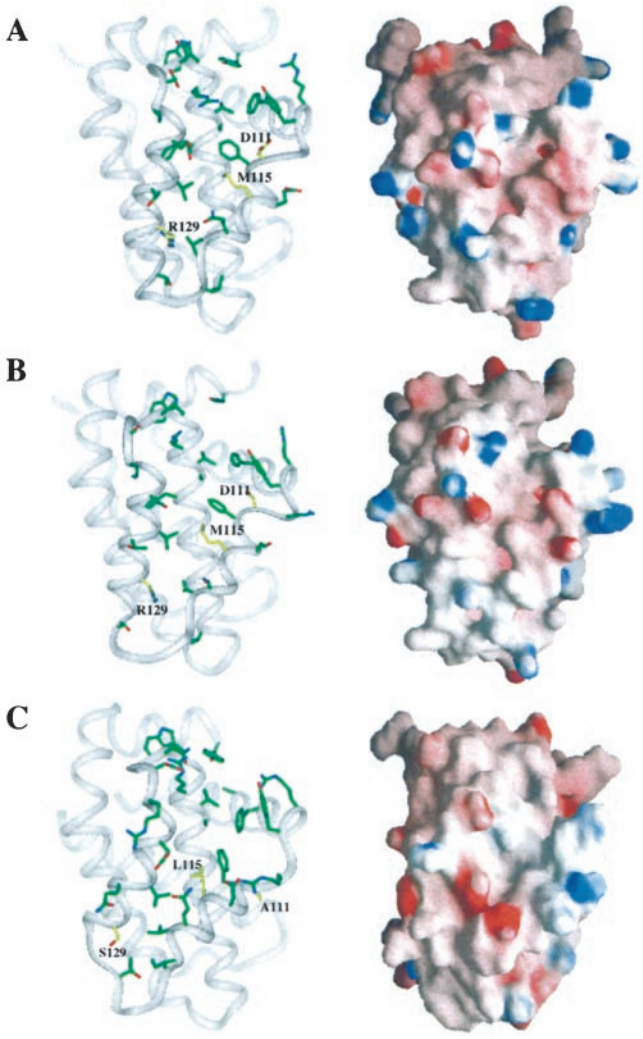

Fig. 4. Binding groove with key side chains and electrostatic [GRASP (45)]) surface for Bcl-2(1) (*A*), Bcl-2(2) (*B*), and Bcl-x_L (*C*). Residues that differ between the Bcl-2 proteins and Bcl-x_L are highlighted in yellow.

between Bcl-2(1) and Bcl-x_L drops to 1.71 Å, and the RMSD between Bcl-2(2) and Bcl-x_L is 1.61 Å. In Bcl-2, this region consists of one turn of a 3_{10} helix rather than the regular α-helix observed in Bcl-x_L. In addition, this region of Bcl-2 along with the first turn of helix 4 is translated with respect to the corresponding region in Bcl-x_L (Fig. 6). This difference most likely is due to hydrophobic contacts in Bcl-x_L between the side chains of

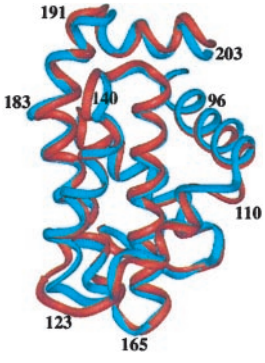

Fig. 5. Backbone superposition of Bcl-2(1) (red) with Bcl-2(2) (blue).

Table 2. Peptide binding to Bcl-2 and Bcl-x_L

Peptide	Sequence	Bcl-2(1) Kd, nM	Bcl-2(2) Kd, nM	Bcl-x_L Kd, nM
Bad 25-mer	NLWAAQRYGRELRRMSDEFVDSFKK	15	8	0.6
Bak 16-mer	GQVGRQLAIIGDDINR	12,710	1,600	480

Tyr-127 in helix 4 and Thr-179 and Tyr-180 in helix 6, which pulls the amino-terminal end of helix 4 toward helix 6. These contacts are not observed in Bcl-2, because residues 127 and 179 are arginine and glutamic acid, respectively.

In addition to the structural differences observed between Bcl-2 and Bcl-x_L in the hydrophobic groove, there are a few key differences in primary sequence that translate into a different topology for the binding groove. The amino acids that differ in this region of the two proteins include: residue 111 (Asp in Bcl-2; Ala in Bcl-x_L), residue 115 (Met in Bcl-2; Leu in Bcl-x_L), and residue 129 (Arg in Bcl-2; Ser in Bcl-x_L). These amino acid differences are highlighted in yellow in Fig. 4. Of these differences, the aspartic-acid-to-alanine and arginine-to-serine substitutions would be expected to change the character of the binding groove the most, since this substitution alters the charge of the protein. A comparison of the GRASP surface of Bcl-x_L (Fig. 4*C*) to that of Bcl-2 (Fig. 4 *A* and *B*) supports this conclusion. There is a concentration of negative potential at the bottom of the groove in Bcl-x_L that is not present in Bcl-2. This negative charge most likely arises from two acidic residues: Asp-114 and Glu-135. In the Bcl-2 proteins, this negative charge is compensated by Arg-129, which is a serine in Bcl-x_L.

This difference in the electrostatic surface of the binding groove could explain, at least in part, the higher affinity of Bcl-x_L for Bad and Bak peptides compared with Bcl-2(1) and Bcl-2(2) (Table 2). In the Bcl-x_L–Bak and Bcl-x_L–Bad peptide complexes (21, 22), the helical peptide was observed to bind with its

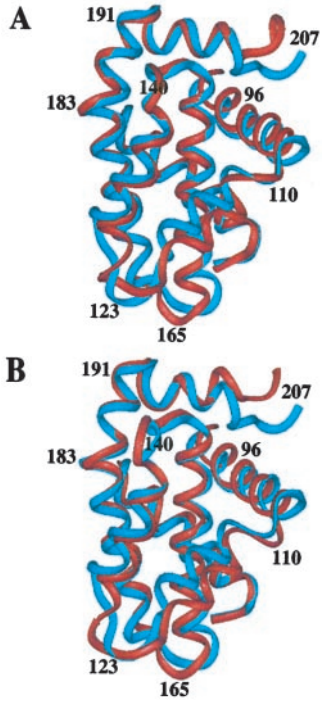

Fig. 6. (*A*) Backbone superposition of Bcl-2(1) (red) with Bcl-x_L (blue). (*B*) Backbone superposition of Bcl-2(2) (red) with Bcl-x_L (blue).

amino-terminal electropositive end toward the bottom of the binding groove. As discussed above, this region is more electronegative in Bcl-x_L compared with Bcl-2, which may account for the higher affinity of these peptides for Bcl-x_L.

Recently, the NMR-derived structure of the proapoptotic protein Bax was reported by Suzuki *et al.* (46) who used a Bax construct with the putative transmembrane region and flexible loop intact. Although Bax plays a very different role in apoptosis compared with Bcl-2 and Bcl-x_L, the overall fold of these proteins is similar. Excluding the transmembrane region, Bax contains the same number of helices as the two antiapoptotic proteins, and the relative orientation of these helices is the same. The RMSD between Bcl-2(1) and Bax is 1.9 Å, whereas the RMSD between Bcl-2(2) and Bax is 2.2 Å. Based on the NMR data, the loop between helix 1 and helix 2 in Bax is largely disordered. Only weak NOEs were observed between the central portion of this loop and two residues on helix 6. This result is consistent with the structure of Bcl-x_L, in which this loop is flexible and suggests that the corresponding loop in Bcl-2 would be disordered also.

Conclusions

The structures of two isoforms of the antiapoptotic protein Bcl-2 have been determined by NMR spectroscopy. A critical aspect of this work was the preparation of soluble monomeric proteins that were amenable to structure determination by NMR. This determination was accomplished by lowering the pI of Bcl-2 by replacing the loop of Bcl-2 with acidic residues found in the loop of Bcl-x_L. The structures of the two Bcl-2 isoforms were found to be very similar. However, the different affinities observed for Bak and Bad peptides suggest that there must be subtle differences in the binding grooves of the two isoforms of Bcl-2. The structure of Bcl-2 differs from Bcl-x_L4 in the binding groove. The third α-helix that makes up an important part of the binding pocket in Bcl-x_L is a 3_{10} helix in Bcl-2. There are differences also in primary sequence in this region of the two proteins. These differences in structure and the amino acids that comprise the binding pocket define the binding specificities observed for Bcl-x_L and Bcl-2. This information could be used to aid in the design of small molecules that bind to Bcl-2 and/or Bcl-x_L and potentially antagonize their function. These small molecules may be useful for the treatment of cancers in which these proteins are overexpressed.

We thank Dr. Rob Meadows for help with the structure calculations and for useful discussions. The member who communicated this paper is on the Scientific Advisory Board of IDUN Pharmaceuticals.

1. Tsujimoto, Y., Finger, L. R., Yunis, J., Nowell, P. C. & Croce, C. M. (1984) *Science* **226,** 1097–1099.
2. Tsujimoto, Y. & Croce, C. M. (1986) *Proc. Natl. Acad. Sci. USA* **83,** 5214–5218.
3. Cleary, M. L. & Sklar, J. (1985) *Proc. Natl. Acad. Sci. USA* **82,** 7439–7443.
4. Cleary, M. L., Smith, S. D. & Sklar, J. (1986) *Cell* **47,** 19–28.
5. Bakhsi, A., Jensen, J. P., Goldman, P., Wright, J. J., McBride, O. W., Epstein, A. L. & Korsmeyer, S. J. (1985) *Cell* **41,** 899–906.
6. Seto, M., Jaeger, U., Hockett, R. D., Graninger, W., Bennett, S., Goldman, P. & Korsmeyer, S. J. (1988) *EMBO J.* **7,** 123–131.
7. Adams, J. M. & Cory, S. (1998) *Science* **281,** 1322–1326.
8. Kelekar, A. & Thompson, C. B. (1998) *Trends Cell Biol.* **8,** 324–330.
9. Chao, D. T. & Korsmeyer, S. J. (1998) *Annu. Rev. Immunol.* **16,** 395–419.
10. Reed, J. C. (1999) *Curr. Opin. Oncol.* **11,** 68–75.
11. Yang, E., Zha, J., Jockel, J., Boise, L. H., Thompson, C. B. & Korsmeyer, S. J. (1995) *Cell* **80,** 285–291.
12. Thompson, C. B. (1995) *Science* **267,** 1456–1462.
13. Kusenda, J. (1998) *Neoplasma (Bratisl.)* **45,** 117–122.
14. Strasser, A., Huang, D. C. S. & Vaux, D. L. (1997) *Biochim. Biophys. Acta* **1333,** F151–F178.
15. Berghella, A. M., Pellegrini, P., Contasta, I., Del Beato, T. & Adorno, D. (1998) *Cancer Biother. Radiopharm.* **13,** 225–236.
16. Nicholson, D. W. (2000) *Nature (London)* **407,** 810–816.
17. Piche, A., Grim, J., Rancourt, C., Gomez-Navarro, J., Reed, J. C. & Curiel, D. T. (1998) *Cancer Res.* **58,** 2134–2140.
18. Wang, J. L., Zhang, Z. J., Choksi, S., Shan, S., Lu, Z., Croce, C. M., Alnemri, E. S., Korngold, R. & Huang, Z. (2000) *Cancer Res.* **60,** 1498–1502.
19. Wang, J. L., Liu, D., Zhang, Z. J., Shan, S., Han, X., Srinvasula, S. M., Croce, C. M., Alnemri, E. S. & Huang, Z. (2000) *Proc. Natl. Acad. Sci. USA* **97,** 7124–7129.
20. Muchmore, S. W., Sattler, M., Liang, H., Meadows, R. P., Harlan, J. E., Yoon, H. S., Nettesheim, D., Chang, B. S., Thompson, C. B., Wong, S. L., *et al.* (1996) *Nature (London)* **381,** 335–341.
21. Sattler, M., Liang, H., Nettesheim, D., Meadows, R. P., Harlan, J. E., Eberstadt, M., Yoon, H. S., Shuker, S. B., Chang, B. S., Minn, A. J., *et al.* (1997) *Science* **275,** 983–986.
22. Petros, A. M., Nettesheim, D. G., Wang, Y., Olejniczak, E. T., Meadows, R. P., Mack, J., Swift, K., Matayoshi, E. D., Zhang, H., Thompson, C. B. & Fesik, S. W. (2000) *Protein Sci.* **9,** in press.
23. Veis, D. J., Sorenson, C. M., Shutter, J. R. & Korsmeyer, S. J. (1993) *Cell* **75,** 229–240.
24. Nakayama, K., Negishi, I., Kuida, K., Sawa, H. & Loh, D. Y. (1994) *Proc. Natl. Acad. Sci. USA* **91,** 3700–3704.
25. Kamada, S., Shimono, A., Shinto, Y., Tsujimura, T., Takahashi, T., Noda, T., Kitamura, Y., Kondoh, H. & Tsujimoto, Y. (1995) *Cancer Res.* **55,** 354–359.
26. Motoyama, N., Wang, F., Roth, K. A., Sawa, H., Nakayama, K., Negishi, I., Senju, S., Zhang, Q., Fujii, S. & Loh, D. Y. (1995) *Science* **267,** 1506–1510.
27. Boise, L. H., Gonzalez-Garcia, M., Postema, C. E., Ding, L., Lindsten, T., Turka, L. A., Mao, X., Nunez, G. & Thompson, C. B. (1993) *Cell* **74,** 597–608.
28. Campos, L., Rouault, J. P., Sabido, O., Oriol, P., Roubi, N., Vasselon, C., Archimbund, E., Magaud, J. P. & Guyotat, D. (1993) *Blood* **81,** 3091–3096.
29. Olopade, O. I., Adeyanju, M. O., Safa, A. R., Hagos, F., Mick, R., Thompson, C. B. & Recant, W. M. (1997) *Cancer J. Sci. Am.* **3,** 230–237.
30. Ottilie, S., Diaz, J. L., Horne, W., Chang, J., Wang, Y., Wilson, G., Chang, S., Weeks, S., Fritz, L. C. & Oltersdorf, T. (1997) *J. Biol. Chem.* **272,** 30866–30872.
31. Yamazaki, T., Lee, W., Arrowsmith, C. H., Muhandiram, D. R. & Kay, L. E. (1994) *J. Am. Chem. Soc.* **116,** 11655–11666.
32. Clore, G. M. & Gronenborn, A. M. (1994) *Methods Enzymol.* **239,** 349–363.
33. Neri, D., Szyperski, T., Otting, G., Senn, H. & Wüthrich, K. (1989) *Biochemistry* **28,** 7510–7516.
34. Fesik, S. W. & Zuiderweg, E. R. P. (1988) *J. Magn. Reson.* **78,** 588–593.
35. Marion, D., Driscoll, P. C., Kay, L. E., Wingfield, P. T., Bax, A., Gronenborn, A. M. & Clore, G. M. (1989) *Biochemistry* **29,** 6150–6156.
36. Tjandra, N. (1999) *Structure (London)* **7,** R205–R211.
37. Hansen, M. R., Mueller, L. & Pardi, A. (1998) *Nat. Struct. Biol.* **5,** 1065–1074.
38. Clore, G. M., Starich, M. R. & Gronenborn, A. M. (1998) *J. Am. Chem. Soc.* **120,** 10571–10572.
39. Brunger, A. T. (1992) X-PLOR Version 3.1 manual (Yale Univ. Press, London).
40. Cornilescu, G., Delaglio, F. & Bax, A. (1999) *J. Biomol. NMR* **13,** 289–302.
41. Laskowski, R. A., MacArthur, M. W., Moss, D. S. & Thornton, J. M. (1993) *J. Appl. Crystallogr.* **26,** 283–291.
42. Dandliker, W. B., Hsu, M. L., Levin, J. & Rao, B. R. (1981) *Methods Enzymol.* **74,** 3–28.
43. Anderson, M., Blowers, D., Hewitt, N., Hedge, P., Breeze, A., Hampton, I. & Taylor, I. (1999) *Protein Expression Purif.* **15,** 162–170.
44. Yin, X. M., Oltvai, Z. N. & Korsmeyer, S. J. (1994) *Nature (London)* **369,** 321–323.
45. Nichols, A. J., Sharp, K. A. & Honig, B. (1991) *Proteins Struct. Funct. Genet.* **11,** 281–296.
46. Suzuki, M., Youle, R. J. & Tjandra, N. (2000) *Cell* **103,** 645–654.
47. Carson, M. (1987) *J. Mol. Graphics* **5,** 103–106.